QUANTUM OPTICS

Observation of three-photon bound states in a quantum nonlinear medium

Qi-Yu Liang,[1] Aditya V. Venkatramani,[2] Sergio H. Cantu,[1] Travis L. Nicholson,[1] Michael J. Gullans,[3,4] Alexey V. Gorshkov,[4] Jeff D. Thompson,[5] Cheng Chin,[6] Mikhail D. Lukin,[2]* Vladan Vuletić[1]*

Bound states of massive particles, such as nuclei, atoms, or molecules, constitute the bulk of the visible world around us. By contrast, photons typically only interact weakly. We report the observation of traveling three-photon bound states in a quantum nonlinear medium where the interactions between photons are mediated by atomic Rydberg states. Photon correlation and conditional phase measurements reveal the distinct bunching and phase features associated with three-photon and two-photon bound states. Such photonic trimers and dimers possess shape-preserving wave functions that depend on the constituent photon number. The observed bunching and strongly nonlinear optical phase are described by an effective field theory of Rydberg-induced photon-photon interactions. These observations demonstrate the ability to realize and control strongly interacting quantum many-body states of light.

Bound states of light quanta have been proposed to exist in specifically engineered media with strong optical nonlinearities (*1*–*5*). In recent times, photonic dimers have been observed experimentally (*6*). Such bound states of photons can be viewed as quantum solitons (*7*, *8*), which are shape-preserving wave packets enabled by the cancellation of nonlinear and dispersive effects. In contrast to classical solitons, where the self-consistent shape varies smoothly with total pulse energy, quantum solitons have optical nonlinearity that is strong enough for the wave packet shape to depend on the constituent number of photons in a quantized manner (*7*, *8*). The creation of quantum solitons not only represents an important step in fundamental studies of photonic quantum matter (*6*, *9*, *10*) but also may enable new applications in areas ranging from quantum communication to quantum metrology (*11*, *12*).

We use an ultracold atomic gas as a quantum nonlinear medium to search for a photonic trimer. This medium is experimentally realized by coupling photons to highly excited atomic Rydberg states by means of electromagnetically induced transparency (EIT). The resulting hybrid excitations of light and matter—Rydberg polaritons—inherit strong interactions from their Rydberg components and can propagate with very low loss at slow group velocity v_g (*13*–*15*). The nonlinearity arises when photons are within a Rydberg blockade radius r_B of one another, where strong interactions between atoms in the Rydberg state (*16*) shift the Rydberg level out of the EIT resonance, blocking the excitation of more than one Rydberg atom within r_B. In the dissipative regime (on atomic resonance), the blockade results in photon loss and antibunching (*17*–*19*). In the dispersive, off-resonant regime, the index of refraction varies with the separation between photons, resulting in an attractive force (*6*).

Our experimental setup (*20*) (Fig. 1, A and B) consists of a weak quantum probe field at wavelength λ = 780 nm and waist w = 4.5 μm coupled to the $100S_{1/2}$ Rydberg state via a strong 479-nm control field in the EIT configuration (Fig. 1B). The interactions occurred in a cloud of laser-cooled ^{87}Rb atoms in a far-detuned optical dipole trap. Measurements are conducted at a peak optical depth $OD_B \simeq 5$ per blockade radius r_B = 20 μm. To suppress dissipative effects, we work at a large detuning $\Delta \geq 3\Gamma$ from atomic resonance (Γ is the population decay rate of the $5P_{3/2}$ state; see Fig. 1B) and at a control laser Rabi frequency where the transmission through the medium is the same with and without EIT, but the phase differs appreciably (Fig. 1C). Consequently, the transmission hardly varies with probe photon rate (Fig. 1D, top), whereas a strongly rate-dependent phase with a slope of 0.40(±0.07) rad·μs is observed (Fig. 1D, bottom).

The quantum dynamics of interacting photons are investigated by measuring the three-photon correlation function and phase. Because dispersion outside of the atomic medium is negligible, any amplitude and phase features formed inside the nonlinear medium are preserved outside and can be detected in the form of photon number and phase correlations. The third-order photon correlation function has been measured previously in coupled atom-cavity and quantum dot–cavity systems, as well as in nonclassical states of three photons such as the Greenberger-Horne-Zeilinger and N00N states (*12*). In our approach, we split the light onto three single-photon counting modules. Furthermore, by mixing a detuned local oscillator into the final beam splitter, we can also perform a heterodyne measurement in one of the detection arms (Fig. 1A). To connect the observed correlations to the physics of interacting Rydberg polaritons, we consider a state containing up to three photons

$$|\psi\rangle = |0\rangle + \int dt_1\, \psi_1(t_1)|t_1\rangle + \int dt_1 dt_2\, \psi_2(t_1,t_2)|t_1,t_2\rangle + \int dt_1 dt_2 dt_3\, \psi_3(t_1,t_2,t_3)|t_1,t_2,t_3\rangle \quad (1)$$

where $|t_1,\cdots,t_N\rangle = \frac{1}{N!}a^\dagger(t_1)\cdots a^\dagger(t_N)|0\rangle$, $a^\dagger(t)$ is the photon creation operator of the time bin mode t, and N is the number of photons. The correlation functions (Fig. 2) can be related to the wave functions as $g^{(2)}(t_1,t_2) = \frac{|\psi_2(t_1,t_2)|^3}{|\psi_1(t_1)|^2|\psi_1(t_2)|^2}$ and $g^{(3)}(t_1,t_2,t_3) = \frac{|\psi_3(t_1,t_2,t_3)|^2}{|\psi_1(t_1)|^2|\psi_1(t_2)|^2|\psi_1(t_3)|^2}$. We refer to the phase $\tilde{\phi}^{(N)}$ of the N-photon wave function ψ_N as the N-photon phase—namely, $\tilde{\phi}^{(1)}(t_1) = \mathrm{Arg}[\psi_1(t_1)]$, $\tilde{\phi}^{(2)}(t_1,t_2) = \mathrm{Arg}[\psi_2(t_1,t_2)]$, and $\tilde{\phi}^{(3)}(t_1,t_2,t_3) = \mathrm{Arg}[\psi_3(t_1,t_2,t_3)]$. The N-photon phase is obtained from the phase of the beat note signal on the third detector, conditioned on having observed $N-1$ photons in the other two detectors. The conditional phase relative to N uncorrelated photons (i.e., the nonlinear part of the phase) is denoted as $\phi^{(N)}$ (Fig. 3).

The experimentally measured $g^{(3)}$ function (Fig. 2, A and B) displays a clear bunching feature: The probability to detect three photons within a short time (≲25 ns) of one another is six times higher than for noninteracting photons in a laser beam. The increase at $t_1 = t_2 = t_3$ is accompanied by a depletion region for photons arriving within ~0.7 μs of one another, particularly visible along the lines of two-photon correlations ($t_i = t_j \neq t_k$, where t_i, t_j, and t_k are the photon detection times at detectors D_i, D_j, and D_k, respectively, and i, j, and k are permutations of 1, 2, and 3) (Fig. 2A): This depletion region is caused by the inflow of probability current toward the center $t_1 = t_2 = t_3$. Figure 2B compares the two-photon correlation function $g^{(2)}(t, t+|\tau|)$ with that for three photons, of which two were detected in the same time bin, $g^{(3)}(t, t, t+|\tau|)$. The trimer feature is approximately a factor of 2 narrower than the dimer feature, showing that a photon is attracted more strongly to two other photons than to one. Figure 2C illustrates the binding of a third photon to two photons that are detected with a time separation T. If T exceeds the dimer time scale τ_2, then the third photon binds independently to either

[1]Department of Physics and Research Laboratory of Electronics, Massachusetts Institute of Technology, Cambridge, MA 02139, USA. [2]Department of Physics, Harvard University, Cambridge, MA 02138, USA. [3]Department of Physics, Princeton University, Princeton, NJ 08544, USA. [4]Joint Quantum Institute and Joint Center for Quantum Information and Computer Science, National Institute of Standards and Technology and University of Maryland, College Park, MD 20742, USA. [5]Department of Electrical Engineering, Princeton University, Princeton, NJ 08544, USA. [6]James Franck Institute, Enrico Fermi Institute, and Department of Physics, University of Chicago, Chicago, IL 60637, USA.
*Corresponding author. Email: lukin@physics.harvard.edu (M.D.L.); vuletic@mit.edu (V.V.)

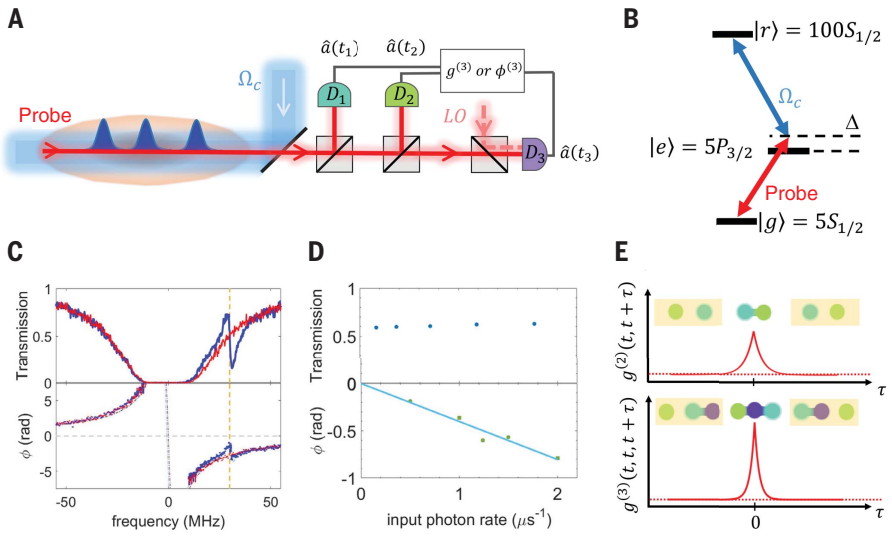

Fig. 1. Qualitative descriptions of the experiment. (**A** and **B**) Setup and atomic-level scheme. The atoms are optically pumped into the hyperfine (F) and magnetic (m_F) sublevel $|g\rangle = |5S_{1/2}, F = 2, m_F = 2\rangle$. The weak coherent probe light is coupled to the Rydberg state $|r\rangle = |100S_{1/2}, m_J = 1/2\rangle$ (m_J, projection of the total electron angular momentum along the quantization axis) via an intermediate state $|e\rangle = |5P_{3/2}, F = 3, m_F = 3\rangle$, with linewidth $\Gamma/2\pi$ = 6.1 MHz, by means of a counterpropagating control field that is detuned by fj below the resonance frequency of the upper transition, $|e\rangle \rightarrow |r\rangle$. Strong interactions between probe photons are detected via photon correlations of the transmitted light, which is split onto three single-photon detectors with equal intensities. To perform phase measurements, a local oscillator is mixed into detector D_3. $\hat{a}(t)$, photon annihilation operator of the time bin mode t; Ω_c, control laser Rabi frequency; g, correlation function; ϕ, phase; LO, local oscillator. (**C**) Transmission (top) and phase ϕ (bottom) as a function of probe frequency measured at a low input photon rate (0.5 μs^{-1}). ϕ is measured without conditioning on the detection of other photons. The control laser is set at $\Delta/2\pi$ = 30 MHz below the $|e\rangle \rightarrow |r\rangle$transition, with Rabi frequency $\Omega_c/2\pi$ = 10 MHz. The blue and red traces are from measurements with and without a control beam, respectively. The blue and red dashed lines in the bottom graph are theoretical expectations. The vertical yellow dashed line marks electromagnetically induced transparency (EIT) resonance. (**D**) Rate dependence of transmission (top) and unconditional phase (bottom) on the two-photon resonance $|g\rangle \rightarrow |r\rangle$, with a one-photon detuning of $\Delta/2\pi$ = 30 MHz and a control Rabi frequency $\Omega_c/2\pi$ = 10 MHz. Whereas the transmission is rate-independent, the phase is strongly rate-dependent (slope is 0.4 rad·μs). (**E**) Schematic correlation functions for two (top) and three (bottom) photons as a function of their time separation τ. The attractive interaction leads to photon bunching, with three photons being more tightly bound together than two photons.

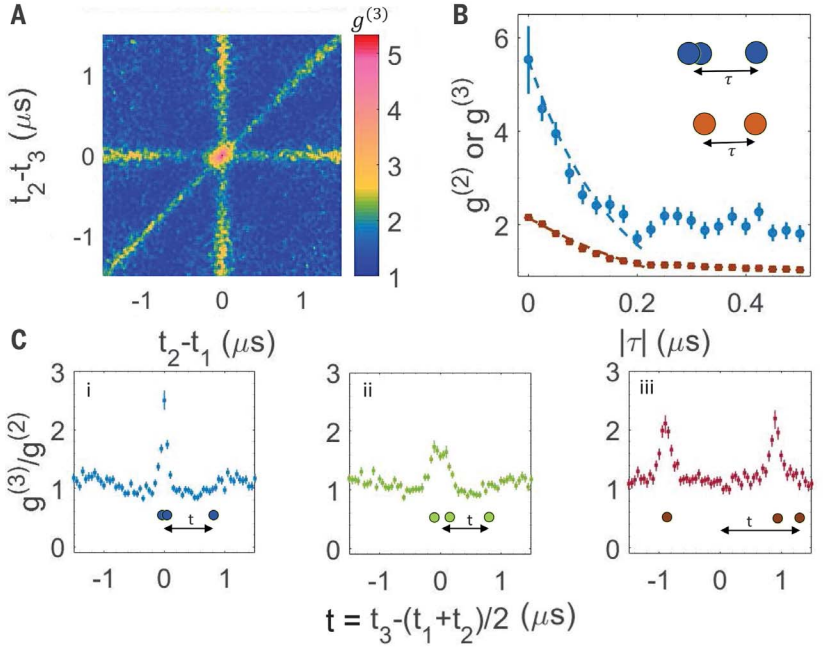

Fig. 2. Photon correlation functions with tighter bunching due to the three-photon bound state. Photon correlation functions were measured on EIT resonance and at one-photon detuning $\Delta/2\pi$ = 30 MHz, control Rabi frequency $\Omega_c/2\pi$ = 10 MHz, an input photon rate of 1 μs^{-1}. (**A**) 2D representation of the three-photon correlation function $g^{(3)}(t_1, t_2, t_3)$, with t_i being the photon detection time at detector D_i. Three-photon bunching corresponds to the central region, two-photon bunching to the stripes. (**B**) $g^{(3)}(t, t, t + |\tau|)$ (blue data points) and $g^{(2)}(t, t + |\tau|)$ (brown data points), with the decay constants calculated from the exact solution for the bound states τ_3^c = 0.16 μs and τ_2^c = 0.32 μs, respectively (dashed lines). The calculated exponential decay is scaled to match the initial point of the measured intensity correlation functions. The approximately twofold smaller decay length of the three-photon correlation function shows that a photon is more strongly bound to two photons than to one. The fitted exponential decay constants with zero offset for $g^{(3)}$ and $g^{(2)}$ are τ_3 = 0.14(2) μs and τ_2 = 0.31(6) μs, respectively, in agreement with the calculated values. (**C**) Three representative plots of $g^{(3)}(t_1, t_2, t_3)/g^{(2)}(t_1, t_2)$ for fixed time separation $T \equiv |t_1 - t_2|$ = 0 μs (i), T = 0.2 μs (ii), and T = 1.8 μs (iii), within a 50-ns window. As the two photons get farther and farther away from each other, the sharply decaying $g^{(3)}$ function transitions to a slower decaying $g^{(2)}$ function. For intermediate time separations (ii), interference occurs between all states, including the dimer and trimer. All permutations of the detectors are used to generate the data in (B) and (C). Error bars indicate 1 SD.

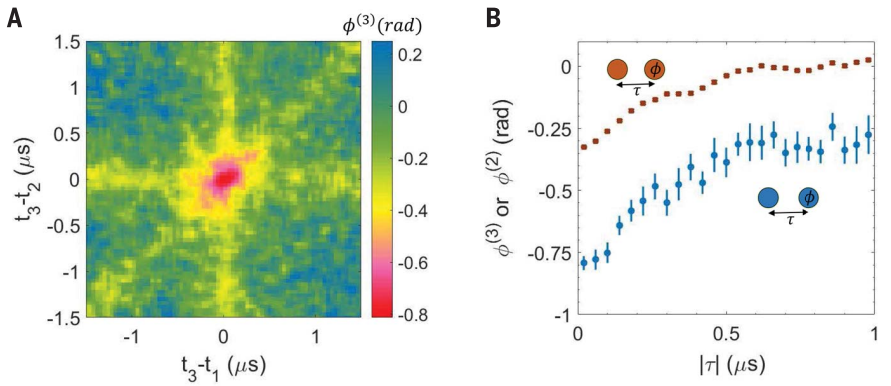

Fig. 3. Larger nonlinear phase for three photons. Nonlinear phase was measured under identical conditions as the data in Fig. 2. (**A**) Conditional phase $\phi^{(3)}(t_1,t_2,t_3)$, where t_1 and t_2 correspond to photon detection events at detectors D_1 and D_2, and a heterodyne measurement is performed on detector D_3 at time t_3. (**B**) Diagonal cut $\phi^{(3)}(t,t,t+|\tau|)$ (blue), with the two conditioning probe photons within 40 ns of each other, and $\phi^{(2)}(t,t+|\tau|)$ (brown), showing a larger phase when conditioning on two other near-simultaneous photons [$\phi^{(3)}$] than on one near-simultaneous photon [$\phi^{(2)}$]. $\phi^{(N)}$ is referenced to its own average value when all N photons are too far apart to be correlated. Specifically, $\phi^{(2)}(t_1,t_2)\equiv\tilde{\phi}^{(2)}(t_1,t_2)-\left(\tilde{\phi}^{(1)}(t_1)+\tilde{\phi}^{(1)}(t_2)\right)\xrightarrow{|t_1-t_2|\to\infty}0$ and $\phi^{(3)}(t_1,t_2,t_3)\equiv\tilde{\phi}^{(3)}(t_1,t_2,t_3)-\left(\tilde{\phi}^{(1)}(t_1)+\tilde{\phi}^{(1)}(t_2)+\tilde{\phi}^{(1)}(t_3)\right)\xrightarrow{|t_i-t_j|\to\infty,\forall i\neq j}0$. At large $|\tau|$, $\phi^{(3)}$ asymptotically goes to $\phi^{(2)}(t,t)$ because $\phi^{(3)}(t,t,t+|\tau|)\xrightarrow{|\tau|\to\infty}\tilde{\phi}^{(2)}(t,t)+\tilde{\phi}^{(1)}(t+|\tau|)-\left(\tilde{\phi}^{(1)}(t)+\tilde{\phi}^{(1)}(t+|\tau|)\right)=\phi^{(2)}(t,t)$. Error bars indicate 1 SD.

photon, whereas for $T<\tau_2$ the two peaks merge into a single, more tightly bound trimer. This is analogous to the binding of a particle to a double-well potential as the distance between the wells is varied, because the polaritons can be approximately described as interacting massive particles moving at a finite group velocity (*6*).

The dispersive and distance-dependent photon-photon interaction also manifests itself in a large conditional phase shift that depends on the time interval τ between the detection of the conditioning photons (at times $t_1=t_2=t$) and the phase measurement on detector D_3 at time t_3. We observe a conditional phase shift $\phi^{(3)}(t,t,t+|\tau|)$ for the trimer near $\tau=0$ (Fig. 3A) that is substantially larger than the dimer phase shift $\phi^{(2)}(t,t+|\tau|)$ (Fig. 3B). This confirms that the interaction between a photon and a dimer is stronger than that between two photons.

To understand these results quantitatively, we apply an effective field theory (EFT) (*21*) that describes the low-energy scattering of Rydberg polaritons. This EFT gives us a one-dimensional (1D) slow-light Hamiltonian density with a contact interaction

$$\mathcal{H}=-\hat{\psi}^{\dagger}\left(i\hbar v_g\frac{\partial}{\partial_z}+\frac{\hbar^2}{2m}\frac{\partial^2}{\partial_z^2}\right)\hat{\psi}-\frac{\hbar^2}{ma}\hat{\psi}^{\dagger 2}\hat{\psi}^2 \quad (2)$$

where v_g is the group velocity inside the medium, $m=-\hbar\Omega_c^2/(8\Delta v_g^2)$ is the effective photon mass, $\hbar$ is Planck's constant h divided by 2π, a is the scattering length, Ω_c is the control laser Rabi frequency, and Δ is the one-photon detuning. For weak interactions, $a\approx 15.28\left(\frac{1}{OD_B}\frac{\Delta}{\Gamma}\right)^2 r_B$ (*21*, *22*). The single-mode, 1D approximation is justified by the small size of the probe waist compared with the blockade radius (r_B), whereas the corresponding Rayleigh range is similar to the atomic cloud size (with both being much larger than r_B). The latter condition implies that the incoming light has small transverse momenta components, whereas the former condition ensures that the dominant scattering occurs colinearly with the probe beam. Combined with the large effective transverse mass in this system (*23*), the residual transverse dynamics arising from interactions are effectively frozen out on the time scale of the experiment (*6*, *15*, *18*, *24*). In the limit where the average longitudinal distance between photons is larger than r_B, such that the low-momentum approximation underlying the EFT is valid, the 1D contact model provides an accurate description whenever $a\gg r_B$, the microscopic range of the two-body potential. For our parameters, we find that this condition is well satisfied as $a\gtrsim 10r_B$. $\hat{\psi}$ is a quantum field annihilation operator, which corresponds to a photon outside the medium and a Rydberg polariton inside. For our blue-detuned probe, the effective mass is negative and the interaction is repulsive. This situation maps onto a system with a positive mass and attractive interaction. The bound states can be determined from the exact solution of this model for finite particle numbers (*25*, *26*), resulting in the correlation functions $g^{(3)}(t_1,t_2,t_3)\propto e^{-\frac{|t_1-t_2|}{a/(2v_g)}}e^{-\frac{|t_2-t_3|}{a/(2v_g)}}e^{-\frac{|t_1-t_3|}{a/(2v_g)}}$ and $g^{(2)}(t_1,t_2)\propto e^{-\frac{|t_1-t_2|}{a/(2v_g)}}$.

In the case $t_1=t_2=t$, we find that $g^{(3)}(t,t,t+|\tau|)\propto e^{-2\frac{|\tau|}{a/(2v_g)}}$, implying that the width of three-photon wave packet [corresponding to $g^{(3)}$] is half that of $g^{(2)}$ for the same experimental conditions, in agreement with experimental observations. We calculate $a/(2v_g)=0.32\,\mu$s for our measured experimental parameters (*27*) and find it to be consistent with data (Fig. 2B, dashed lines). Following the quantum quench at the entry of the medium, the initial state is decomposed into the bound state and the continuum of scattering states (*6*). Near $\tau=0$, the scattering states dephase with each other, whereas the bound state propagates without distortion (*27*). This leads to a small contribution of scattering states in this region, with the bound state dominating the $g^{(3)}$ function. The observed value of $g^{(3)}(0)$ is not universal, as it is affected by the contributions from long-wavelength scattering states and nonlinear losses in the system and therefore depends on the atomic density profile of the medium. The dimer and trimer binding energies can be estimated as $E_2=-\frac{\hbar^2}{ma^2}=h\times 0.2\,\mathrm{MHz}$ and $E_3=4E_2$, respectively. This binding energy is ~10^{10} times smaller than in diatomic molecules such as NaCl and H_2 but is comparable to Feshbach (*28*) and Efimov (*29*) bound states of atoms with similar mass m and scattering length a. To further characterize the three-photon bound state, we consider the phase ratio $\phi^{(3)}/\phi^{(2)}$. For the bound-state contribution to the conditional phase $\phi^{(3)}(t,t,t)\left(\phi^{(2)}(t,t)\right)$, the Hamiltonian of Eq. 2 predicts a phase that equals the trimer binding energy multiplied by the propagation time in the medium. Thus, from the bound-state contributions, one would expect a ratio $\phi^{(3)}/\phi^{(2)}=4$, independent of the atom-light detuning Δ. Although the observed ratio (Fig. 4B) is approximately constant, it is smaller than 4.

The observed deviation is probably due to the two contributions of comparable magnitude. One correction arises from the scattering states, or equivalently, from the fact that our Rydberg medium (~130 μm) is comparable in size to the two-photon bound state (~280 μm). For a medium that is short compared with the bound state, one expects the ratio to be 3, consistent with a dispersionless Kerr medium (*30*). The other, more fundamental, correction may be due to a contribution that does not arise from pairwise interactions, effectively representing a three-photon force. Specifically, when all three photons are within one blockade radius of one another, there can be only one Rydberg excitation, and the potential cannot exceed the value corresponding to that of two photons (*21*, *31*). This saturation effect manifests itself as a short-range repulsive effective three-photon force that, according to our theoretical analysis (*27*), results in a reduction of $\phi^{(3)}/\phi^{(2)}$ below 3. The corresponding correction to the bound state is smaller in the weakly interacting regime relevant to these experiments (*31*). This explains why the effective three-photon force has a relatively weak effect on the bunching of $g^{(3)}(|\tau|<0.2\,\mu\mathrm{s})$, which is dominated by the bound state. Both the scaling arguments and numerical evidence indicate that the effective three-photon force contributes to the three-body scattering amplitudes more strongly than two-body finite range effects in this regime (*21*).

To quantitatively understand these effects, the EFT is modified to include the estimated

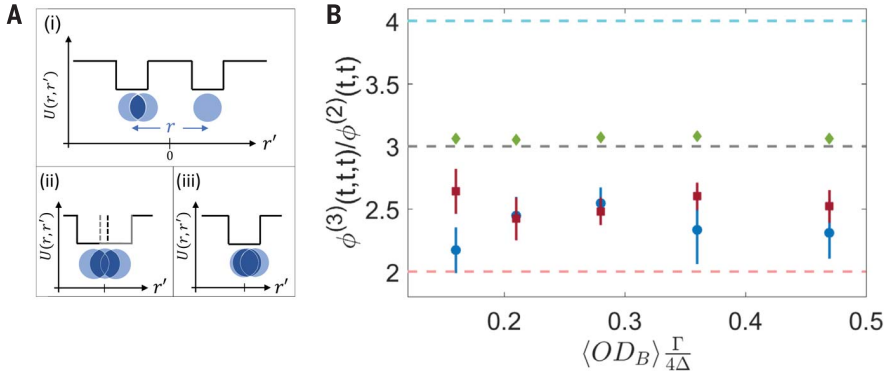

Fig. 4. Comparison of the phase ratio with the effective field theory (EFT) predictions. (**A**) Potential (solid black and gray lines) that the third photon, at position r', experiences because of the other two photons, at positions $\pm r/2$. (i) When the two photons are separated by more than twice the blockade radius ($r > 2r_B$), each of them creates its own square potential with a width of $2r_B$. (ii) When the two photons overlap ($r_B < r < 2r_B$), the potential is partially saturated. Dashed lines denote the overlap of the two interaction potentials. (iii) When the two photons are within one blockade radius ($r < r_B$), because there can be no more than one Rydberg excitation within r_B, the potential is not deeper than that created by one photon. Therefore, we overestimate the attractive potential by considering pairwise interaction only, and a repulsive effective three-photon force is required to correctly account for the saturation of the Rydberg blockade. U, interaction potential between two photons. (**B**) Measured phase ratio $\phi^{(3)}(t,t,t)/\phi^{(2)}(t,t)$ (blue) and EFT predictions (with the effective three-photon force in red; without in green) as a function of $\langle OD_B \rangle \frac{\Gamma}{4\Delta}$, where $\langle\rangle$ refers to the average over the Gaussian profile of the atomic density, and OD_B is optical depth per blockade radius. The quantity $\langle OD_B \rangle \frac{\Gamma}{4\Delta}$ is a quantitative measure of the interaction strength in this system. The control Rabi frequency $\Omega_c/2\pi$ = {22, 18, 10, 10, 8} MHz for $\Delta/2\pi$ = {54, 42, 30, 24, 18} MHz is chosen such that the transmission is insensitive to the input photon rate (Fig. 1C). We also change the input photon rate to {0.7, 1, 1, 1.3, 2.5} photons/μs to achieve similar data-acquisition rates, because the losses are larger at smaller detunings. For a fully saturated medium, one expects $\phi^{(3)}/\phi^{(2)} = 2$, as indicated by the pink dashed line. For bound states in a long medium and no effective three-photon force, one expects $\phi^{(3)}/\phi^{(2)} = 4$, as indicated by the light blue dashed line (see text). For a dispersionless Kerr medium, one expects $\phi^{(3)}/\phi^{(2)} = 3$, as indicated by the gray dashed line. EFT results are calculated with parameters from independent measurements, and the two-photon detuning from the EIT resonance is the only parameter varied within the experimental uncertainty to fit the two-photon phase. Error bars in the EFT with the effective three-photon force arise from the variations with the choice of matching conditions for the three-body scattering amplitudes (*27*). Error bars in the experimental data indicate 1 SD.

effective three-photon force (*27*). Using the modified EFT, we compare the results with and without the repulsive effective three-photon force while also taking into account the effects due to finite medium (Fig. 4B). Including this three-photon saturation force allows the phase ratio $\phi^{(3)}/\phi^{(2)}$ to go below 3, in a reasonable agreement with the experimental observations. For fully saturated interactions between the polaritons, the interaction potential does not increase with photon number, and the phase ratio should approach 2.

The observation of the three-photon bound state, which can be viewed as photonic solitons in the quantum regime (*7*, *8*), can be extended along several different directions. First, increasing the length of the medium at constant atomic density would remove the effect of the scattering states through destructive quantum interference to larger τ and would retain only the solitonic bound-state component. Additionally, the strong observed rate dependence of $\phi^{(3)}$ may indicate that larger photonic molecules and photonic clusters could be observed with improved detection efficiency and data-acquisition rate. Furthermore, with the use of an elliptical or larger round probe beam and careful engineering of the mass along different directions, the system can be extended to two and three dimensions, possibly permitting the observation of photonic Efimov states (*32*, *33*). Finally, our medium supports only one two- or three-photon bound state, corresponding to a nonlinear phase less than π. A threefold increase in the atomic density would render the interaction potential sufficiently deep for a second bound state to appear near zero energy, which should result in resonant photon-photon scattering and a tunable scattering length (*22*). The presence of large effective N-body forces in this system opens avenues to study exotic many-body phases of light and matter, including self-organization in open quantum systems (*34*, *35*) and quantum materials that cannot be realized with conventional systems.

REFERENCES AND NOTES

1. I. H. Deutsch, R. Y. Chiao, J. C. Garrison, *Phys. Rev. Lett.* **69**, 3627–3630 (1992).
2. J.-T. Shen, S. Fan, *Phys. Rev. Lett.* **98**, 153003 (2007).
3. P. Drummond, H. He, *Phys. Rev. A* **56**, R1107–R1109 (1997).
4. Z. Cheng, G. Kurizki, *Phys. Rev. Lett.* **75**, 3430–3433 (1995).
5. Y. Shen, J.-T. Shen, *Phys. Rev. A* **92**, 033803 (2015).
6. O. Firstenberg *et al.*, *Nature* **502**, 71–75 (2013).
7. P. D. Drummond, R. M. Shelby, S. R. Friberg, Y. Yamamoto, *Nature* **365**, 307–313 (1993).
8. Y. Lai, H. A. Haus, *Phys. Rev. A* **40**, 854–866 (1989).
9. D. Chang *et al.*, *Nat. Phys.* **4**, 884–889 (2008).
10. M. F. Maghrebi *et al.*, *Phys. Rev. A* **91**, 033838 (2015).
11. L. Li, A. Kuzmich, *Nat. Commun.* **7**, 13618 (2016).
12. J.-W. Pan *et al.*, *Rev. Mod. Phys.* **84**, 777–838 (2012).
13. I. Friedler, D. Petrosyan, M. Fleischhauer, G. Kurizki, *Phys. Rev. A* **72**, 043803 (2005).
14. D. Petrosyan, J. Otterbach, M. Fleischhauer, *Phys. Rev. Lett.* **107**, 213601 (2011).
15. A. V. Gorshkov, J. Otterbach, M. Fleischhauer, T. Pohl, M. D. Lukin, *Phys. Rev. Lett.* **107**, 133602 (2011).
16. H. Labuhn *et al.*, *Nature* **534**, 667–670 (2016).
17. Y. O. Dudin, A. Kuzmich, *Science* **336**, 887–889 (2012).
18. T. Peyronel *et al.*, *Nature* **488**, 57–60 (2012).
19. D. Maxwell *et al.*, *Phys. Rev. Lett.* **110**, 103001 (2013).
20. J. D. Thompson *et al.*, *Nature* **542**, 206–209 (2017).
21. M. J. Gullans *et al.*, *Phys. Rev. Lett.* **117**, 113601 (2016).
22. P. Bienias *et al.*, *Phys. Rev. A* **90**, 053804 (2014).
23. M. Fleischhauer, J. Otterbach, R. G. Unanyan, *Phys. Rev. Lett.* **101**, 163601 (2008).
24. S. Sevinçli, N. Henkel, C. Ates, T. Pohl, *Phys. Rev. Lett.* **107**, 153001 (2011).
25. E. H. Lieb, W. Liniger, *Phys. Rev.* **130**, 1605–1616 (1963).
26. J. B. McGuire, *J. Math. Phys.* **5**, 622–636 (1964).
27. Supplementary materials are available online.
28. C. Chin, R. Grimm, P. Julienne, E. Tiesinga, *Rev. Mod. Phys.* **82**, 1225–1286 (2010).
29. E. Braaten, H.-W. Hammer, *Ann. Phys.* **322**, 120–163 (2007).
30. P. Bienias, H. P. Büchler, *New J. Phys.* **18**, 123026 (2016).
31. K. Jachymski, P. Bienias, H. P. Büchler, *Phys. Rev. Lett.* **117**, 053601 (2016).
32. M. J. Gullans *et al.*, *Phys. Rev. Lett.* **119**, 233601 (2017).
33. T. Kraemer *et al.*, *Nature* **440**, 315–318 (2006).
34. N. Thaicharoen, A. Schwarzkopf, G. Raithel, *Phys. Rev. Lett.* **118**, 133401 (2017).
35. P. Schauß *et al.*, *Nature* **491**, 87–91 (2012).

ACKNOWLEDGMENTS

We thank O. Firstenberg for help with the early stages of this work and S. Choi for discussions. M.J.G. and A.V.G. thank H. P. Büchler for many insightful discussions and comments on the theoretical analysis. This work has been supported by the NSF, the NSF Center for Ultracold Atoms, the U.S. Army Research Office (ARO), the U.S. Air Force Office of Scientific Research, the ARO Multidisciplinary University Research Initiative, and a Bush Fellowship. A.V.G. and M.J.G. acknowledge additional support by the U.S. Army Research Laboratory Center for Distributed Quantum Information, the NSF Quantum Information Science program, and the NSF Physics Frontiers Center at the Joint Quantum Institute. C.C. acknowledges funding support from NSF grant PHY-1511696 and the Alexander von Humboldt Foundation. All data needed to evaluate the conclusions in the paper are present in the paper and the supplementary materials.

SUPPLEMENTARY MATERIALS

www.sciencemag.org/content/359/6377/783/suppl/DC1
Materials and Methods
Supplementary Text
Figs. S1 to S4
Tables S1 and S2
References (*36*–*40*)

20 August 2017; accepted 4 January 2018
10.1126/science.aao7293

Observation of three-photon bound states in a quantum nonlinear medium

Qi-Yu Liang, Aditya V. Venkatramani, Sergio H. Cantu, Travis L. Nicholson, Michael J. Gullans, Alexey V. Gorshkov, Jeff D. Thompson, Cheng Chin, Mikhail D. Lukin and Vladan Vuletic

Science **359** (6377), 783-786.
DOI: 10.1126/science.aao7293

Forming photonic bound states

Photons do not naturally interact with each other and must be coaxed into doing so. Liang *et al.* show that a gas of Rydberg atoms—a cloud of rubidium atoms excited by a sequence of laser pulses—can induce strong interactions between propagating photons. The authors could tune the strength of the interaction to make the photons form dimer and trimer bound states. This approach should prove useful for producing novel quantum states of light and quantum entanglement on demand.

Science, this issue p. 783